

Article

The Deoxygenation Pathways of Palmitic Acid into Hydrocarbons on Silica-Supported Ni₁₂P₅ and Ni₂P Catalysts

Wenjun Zhou ¹, Hui Xin ², Huiru Yang ¹, Xiangze Du ¹, Rui Yang ¹, Dan Li ^{1,*} and Changwei Hu ^{1,2,*}

¹ Key Laboratory of Green Chemistry and Technology, Ministry of Education, College of Chemistry, Sichuan University, Chengdu 610064, Sichuan, China; Wenjunzhou1993@163.com (W.Z.); YHR15282934710@163.com (H.Y.); xiangzedu95@163.com (X.D.); ruiyang1101@163.com (R.Y.)

² College of Chemical Engineering, Sichuan University, Chengdu 610065, Sichuan, China; Xinhui0327@163.com

* Correspondence: danli@scu.edu.cn (D.L.); changwei.hu@scu.edu.cn (C.H.); Tel.: +86-28-8541-1105 (C.H.)

Received: 3 March 2018; Accepted: 7 April 2018; Published: 11 April 2018



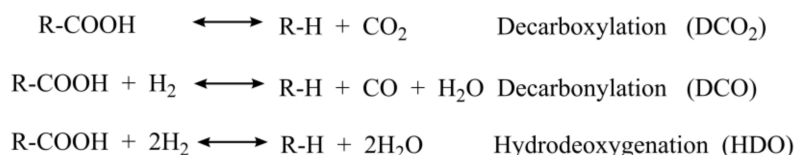
Abstract: Pure Ni₁₂P₅/SiO₂ and pure Ni₂P/SiO₂ catalysts were obtained by adjusting the Ni and P molar ratios, while Ni/SiO₂ catalyst was prepared as a reference against which the deoxygenation pathways of palmitic acid were investigated. The catalysts were characterized by N₂ adsorption, X-ray diffraction (XRD), X-ray photoelectron spectroscopy (XPS), transmission electron microscopy (TEM), infrared spectroscopy of pyridine adsorption (Py-IR), H₂-adsorption and temperature-programmed desorption of hydrogen (H₂-TPD). The crystallographic planes of Ni(111), Ni₁₂P₅(400), Ni₂P(111) were found mainly exposed on the above three catalysts, respectively. It was found that the deoxygenation pathway of palmitic acid mainly proceeded via direct decarboxylation (DCO₂) to form C15 on Ni/SiO₂. In contrast, on the Ni₁₂P₅/SiO₂ catalyst, there were two main competitive pathways producing C15 and C16, one of which mainly proceeded via the decarbonylation (DCO) to form C15 accompanying water formation, and the other pathway produced C16 via the dehydration of hexadecanol intermediate, and the yield of C15 was approximately twofold that of C16. Over the Ni₂P/SiO₂ catalyst, two main deoxygenation pathways formed C15, one of which was mainly the DCO pathway and the other was dehydration accompanying the hexadecanal intermediate and then direct decarbonylation without water formation. The turn over frequency (TOF) followed the order: Ni₁₂P₅/SiO₂ > Ni/SiO₂ > Ni₂P/SiO₂.

Keywords: palmitic acid; nickel phosphide catalysts; deoxygenation pathway; high-index crystal

1. Introduction

Research on alternative resources for hydrocarbon fuel has received wide attention due to diminishing fossil fuel reserves and the environmental crisis during the past decades [1–6]. Furthermore, hydrocarbon fuel from biomass can directly substitute for that from coal, natural gas and petroleum in the current energy system. Biomass-based oil is abundant, and it has the potential to significantly displace petroleum in the production of fuels for the transportation sector. Recently, Richard et al. reported that biofuel blending reduced particle emissions from aircraft engines at cruise condition [7]. Therefore, increased attention has been focused on biomass conversion into hydrocarbon fuel [8–15]. Palmitic acid from palm oil has often been chosen as model compound to investigate the conversion pathway into hydrocarbon fuel by deoxygenation. Currently, three approaches have been used to remove oxygen from fatty acids, that is, decarboxylation (DCO₂), decarbonylation (DCO) and hydrodeoxygenation (HDO) as shown in Scheme 1 [3,15–18], where the degree of H₂ consumption follows the order of DCO₂ < DCO < HDO. Among the three routes, the HDO pathway was characterized by the sequential

reductions of oxygenates to a saturated hydrocarbon, with oxygen being removed as water and the number of carbon atoms being retained in the whole reaction sequence. DCO₂ and DCO pathways removed oxygen by the formation of carbon oxides, which would decrease the number of carbon atoms of the reactant. DCO₂ and DCO pathways were denoted as “carbon-loss reactions” (CLR) [19].



Scheme 1. Possible deoxygenation reactions for fatty acid conversion.

In fact, catalytic deoxygenation of fatty acid and bio-oil has been widely investigated in the past few decades [2,20–23]. Researchers have attempted heterogeneous catalysis to convert fatty acids and their derivatives to fuel-range hydrocarbons. Murzin and co-workers reported that noble metal catalysts exhibited high activity and selectivity for fatty acid conversion [24]. Pd favored CO₂ formation by direct DCO₂, while Pt preferentially promoted the formation of CO by direct DCO [20,22,25]. Ru-based catalysts were also reported to catalyze the cleavage of the C–C bond, DCO and hydrogenolysis during the deoxygenation of acids [26–28]. Furthermore, the deoxygenation of acids over Pd, Pt, Rh, Ru and Ni catalysts mainly proceeded through DCO or DCO₂ with the order of catalytic activity: Pd > Ru > Pt > Rh > Ni [29].

Due to the high price of noble metal catalysts, many researchers have investigated bio-based oil deoxygenation using low-cost catalysts such as Ni, Mo, W, Co-based catalysts from an economic viewpoint [19,30–34]. Peng et al. [25,35] reported that the hydrogenation of the carboxylic group of fatty acid led to the formation of aldehyde catalyzed either solely by metallic Ni or synergistically by Ni and ZrO₂ via ketene as intermediate on Ni/ZrO₂ catalyst, and followed by DCO of octadecanal to the n-heptadecane and carbon monoxide.

Ni and Ni₃S₂ catalysts resulted in DCO₂ hydrocarbon products, while HDO hydrocarbon products formed over Mo, MoS₂ catalysts [19,34,36,37]. Both CoMo and NiMo sulfide catalysts were efficient for deoxygenation by dehydration and DCO reactions [36,37]. NiW catalyst showed a greater tendency towards DCO₂ and DCO compared to NiMo, CoMo and CoMo sulfided catalysts [36,38]. Nevertheless, the sulfide catalysts suffered from deactivation due to sulfur loss, which made researchers begin to focus on non-sulfide catalysts [39,40]. Transition metal phosphides exhibited particular deoxygenation activity, which were considered as a viable substitute to sulfide catalysts for HDO [2,41]. It was reported that the catalyst activity followed the order: Ni₂P > MoP > CoP-Co₂P > WP > Fe₂P-FeP, and the main deoxygenation route was the DCO pathway over metallic Ni, as well as Ni, Co and Fe phosphides, whereas HDO was the main deoxygenation pathway on MoP and WP [30–32]. In comparison to the conventional NiMo/γ-Al₂O₃ catalyst, Ni₂P/SiO₂ had higher activities and showed a promising application for HDO [32,33]. However, nickel phosphides have different crystal forms, such as Ni₁₂P₅, Ni₂P and so on, which might exhibit different catalytic performance in the conversion of bio-based oil. Although several research works have used Ni₂P catalyst for the conversion of palmitic oil to alkane, the detailed mechanisms have not yet been clearly established; in particular, the possibly different performance between Ni₁₂P₅ and Ni₂P catalysts needs more attention.

The aim of this work is to study the deoxygenation mechanism of palmitic acid on Ni₁₂P₅/SiO₂ and Ni₂P/SiO₂ catalysts with an emphasis on their different performance. To better understand the hydrodeoxygenation mechanism of palmitic acid, the reactivity of the main reaction intermediates, such as hexadecanol and hexadecanal, were also comparatively studied for the above catalysts. To eliminate the potential interference of a support, SiO₂ was selected as the support due to its extremely stable physical structure and inert response to the fatty acid hydrodeoxygenation reaction.

2. Results and Discussion

2.1. Characterization of the Catalysts

2.1.1. Ni and P Elemental Analysis

The nickel and phosphorus contents for reduced catalysts determined by inductively coupled plasma (ICP) atomic emission spectroscopy (AES) are shown in Table 1. Ni₂P formed on the SiO₂ and only 10.19% nickel loaded on the SiO₂, which was the lowest among those three catalysts. Ni₁₂P₅ appeared on the SiO₂ with 18.84% nickel loaded. It was noted that the actual nickel loading was in agreement with the controlled loading for pure Ni/SiO₂ catalyst. In this work, the nickel controlled loading was fixed at 24.20% in all catalysts based on our previous study [6]. In fact, the actual nickel loading on SiO₂ was less than the controlled loading and the mass of P was excessive for Ni₁₂P₅/SiO₂ and Ni₂P/SiO₂ catalysts. From the above results, we might think that the mass of P might impact the actual mass of Ni loaded on the SiO₂.

Table 1. The mass fraction of Ni and P for Ni/SiO₂, Ni₁₂P₅/SiO₂ and Ni₂P/SiO₂ catalysts from inductively coupled plasma (ICP) atomic emission spectrometry (AES) (wt %).

Element	Ni	Ni ₁₂ P ₅	Ni ₂ P
Ni	24.20	18.84	10.19
P	-	5.91	10.53

2.1.2. X-ray Diffraction (XRD) and X-ray Photoelectron Spectroscopy (XPS) Results

Figure 1 presents the X-ray diffraction (XRD) patterns of the Ni/SiO₂, Ni₂P/SiO₂ and Ni₁₂P₅/SiO₂ catalysts. For the Ni/SiO₂ catalyst, the three obvious diffraction peaks at 44.4°, 51.7° and 76.4° (PDF#04-0850) were attributed to the metal Ni. For the Ni₁₂P₅/SiO₂ catalyst, the XRD patterns showed only the diffraction peaks at 38.3°, 41.6°, 44.3°, 46.8° and 48.8° assigned to Ni₁₂P₅ (PDF#22-1190). For the Ni₂P/SiO₂ catalyst, the sharp diffraction peaks at 40.7°, 44.5°, 47.2° and 54.8° were assigned to Ni₂P (PDF#03-0953). The crystallite sizes of Ni, Ni₂P, Ni₁₂P₅ were calculated using the Scherrer Equation, and the results are shown in Table 2. Accordingly, the average crystallite sizes of Ni, Ni₂P and Ni₁₂P₅ were 15.6, 36.7 and 17.3 nm, respectively. The crystallite size of Ni₂P was the biggest among these catalysts, which suggested that crystallite Ni₂P easily aggregated into bigger particles compared to Ni and Ni₁₂P₅. It should be noted that no diffraction peaks assigned to Ni₂P were observed on the Ni₁₂P₅/SiO₂ catalyst, meanwhile no diffraction peaks assigned to Ni₁₂P₅ were observed on the Ni₂P/SiO₂ catalyst, indicating the pure phase Ni₂P and Ni₁₂P₅ active component catalysts were obtained.

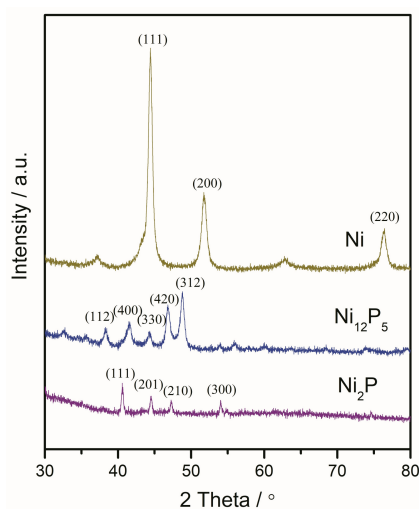
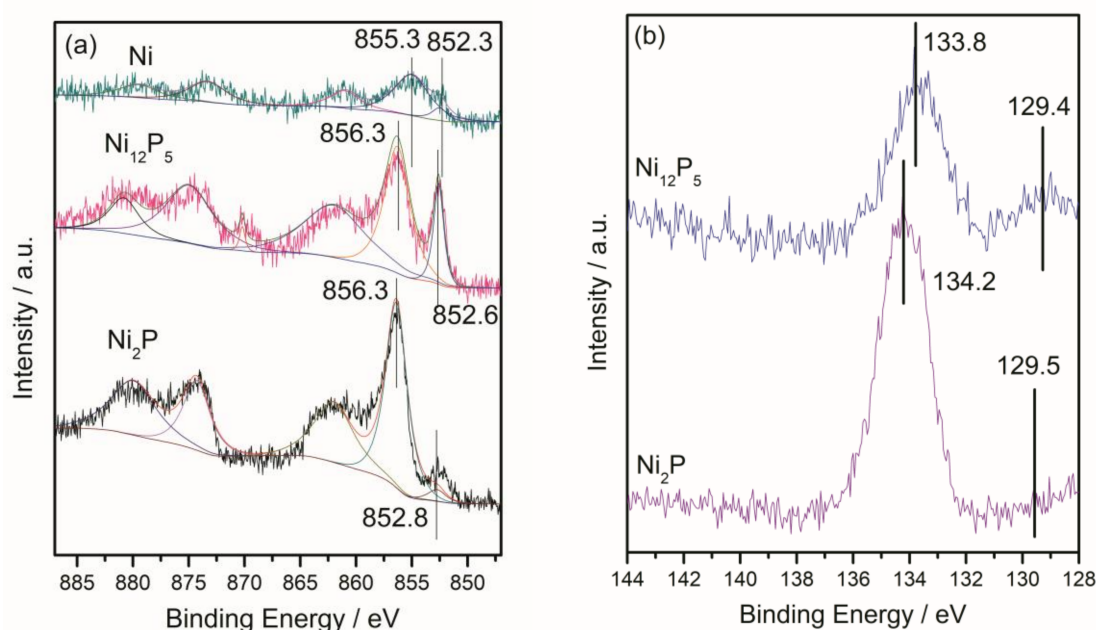


Figure 1. X-ray diffraction (XRD) patterns for the Ni/SiO₂, Ni₁₂P₅/SiO₂ and Ni₂P/SiO₂ catalysts. Intensity is given in arbitrary units (a.u.).

Table 2. Physicochemical and turn over frequency (TOF) data of the samples.

Catalysts	Brunauer–Emmett–Teller (BET) Surface Area ($\text{m}^2 \cdot \text{g}^{-1}$)	Pore Volume ($\text{cm}^3 \cdot \text{g}^{-1}$)	Pore Size (nm)	Crystal Size (nm)	Metal Exposed (%)	Active Site ($\text{mmol} \cdot \text{g}^{-1}$)	TOF (h^{-1})
SiO ₂	342	0.95	11.0	-	-	-	-
Ni/SiO ₂	237	0.66	11.0	15.6	0.34	0.03	468
Ni ₁₂ P ₅ /SiO ₂	218	0.55	10.0	17.3	0.45	0.03	828
Ni ₂ P/SiO ₂	88	0.38	18.6	36.7	0.26	0.02	36

The X-ray photoelectron spectroscopy (XPS) spectra in the Ni (2p) regions for the Ni/SiO₂, Ni₁₂P₅/SiO₂ and Ni₂P/SiO₂ catalysts are shown in Figure 2a and the XPS spectra in the P (2p) regions for the Ni₁₂P₅/SiO₂, Ni₂P/SiO₂ catalysts are shown in Figure 2b. All spectra were decomposed by considering the spin-orbit splitting of the Ni (2p_{3/2}) and Ni (2p_{1/2}) lines (17 eV) and the shake-up peaks at approximately 5 eV higher than the binding energy of the parent signal. For the Ni/SiO₂ catalyst, the peak at approximate 852.3 eV was assigned to Ni metal. For the Ni₁₂P₅/SiO₂ catalyst, the peaks at approximate 856.3 eV and 133.8 eV were assigned to Ni²⁺ and P⁵⁺ species in PO₄³⁻, respectively [42]. The peaks observed at 852.6 eV and 129.4 eV were attributed to reduced Ni^{δ+} ($0 < \delta < 2$) and P species, respectively [43]. As for the Ni₂P/SiO₂ catalyst, the Ni (2p_{3/2}) peaks at 852.8 eV was assigned to Ni^{δ+} in Ni₂P ($0 < \delta < 2$) [43]. The magnitude of δ followed the sequence: Ni₂P > Ni₁₂P₅. The above results were in good agreement with the shift of binding energies detected in references for Ni₂P and Ni₁₂P₅ [42,44].

**Figure 2.** X-ray photoelectron spectroscopy (XPS) spectra in the Ni (2p) regions (a) and P (2p) regions (b) for Ni/SiO₂, Ni₁₂P₅/SiO₂ and Ni₂P/SiO₂.

2.1.3. Textural Properties

The isotherms of N₂ physisorption and pore distribution of the Ni/SiO₂, Ni₁₂P₅/SiO₂ and Ni₂P/SiO₂ catalysts and the support SiO₂ are presented in Figure 3, while the Brunauer–Emmett–Teller (BET) surface areas and other parameters are summarized in Table 2. All the samples possessed type IV sorption isotherms, as shown in Figure 3a. SiO₂ support was mesoporous with pore diameters of approximate 11.0 nm. Both the BET surface areas and the pore volumes of the catalysts decreased compared to SiO₂ support, whereas the average pore diameter of the Ni/SiO₂ and Ni₁₂P₅/SiO₂

catalysts were similar to that of the SiO₂ support. However, the Ni₂P/SiO₂ catalyst suffered a severe loss of surface area and pore volumes. It was found that the small pores ($d < 10$ nm) of Ni₂P/SiO₂ disappeared in Figure 3b. Combined with the P mass fraction from XPS in Table 3 and the high peak of P⁵⁺ species in PO₄³⁻ observed from the XPS spectra in Figure 2b, we speculated that the deposition of phosphorous excess blocked the small pores, which hampered the access of N₂ molecules [45–47]. Nonetheless, excess phosphorous was reported to be necessary for the formation of Ni₂P and maintained Ni₂P particles fully phosphided during reaction progress [42].

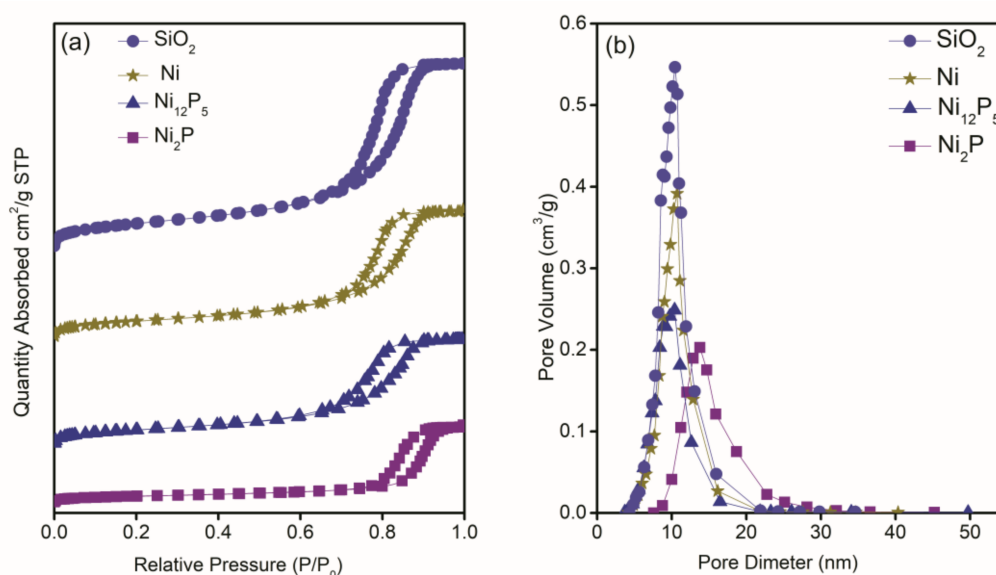


Figure 3. Nitrogen adsorption–desorption isotherm (a) and the Barrett–Joyner–Halenda (BJH) pore-size distribution curve (b) of all samples.

Table 3. The Ni and P mass fraction of Ni/SiO₂, Ni₁₂P₅/SiO₂ and Ni₂P/SiO₂ catalysts from XPS.

Element	Ni	Ni ₁₂ P ₅	Ni ₂ P
Ni	2.82	5.22	4.02
P	-	2.06	5.27
O	54.93	56.90	57.12
Si	42.25	35.82	33.59

2.1.4. H₂-Chemisorption Measurements

The H₂ chemisorption capacities for the reduced catalysts provide the number of surface nickel atoms and an estimate of the active sites. According to the H uptakes at the room temperature for the nickel phosphide catalysts, the exposed metal sites and the active sites are estimated in Table 2. The metal dispersion followed the sequence of Ni₁₂P₅/SiO₂ > Ni/SiO₂ > Ni₂P/SiO₂, and the metal site concentration also followed this sequence.

2.1.5. Transmission Electron Microscopy (TEM)

The low-resolution images revealed the dispersion of the Ni, Ni₁₂P₅ and Ni₂P particles on the SiO₂ supports, as shown in Figure 4. For the Ni/SiO₂ and Ni₂P/SiO₂ catalysts, the Ni and Ni₂P crystallites exhibited poor dispersion. In contrast, the Ni₁₂P₅/SiO₂ catalyst exhibited a spherical shape with good dispersion on SiO₂ support, presumably due to the presence of Ni₁₂P₅ [48]. The above results suggested that Ni₂P and Ni were in favor of aggregation. The high-resolution images of Ni/SiO₂, Ni₁₂P₅/SiO₂ and Ni₂P/SiO₂ revealed that Ni, Ni₁₂P₅ and Ni₂P adopted a globular morphology on the SiO₂ supports. Therefore, a clear difference of crystal indices could be observed among Ni, Ni₁₂P₅ and

Ni_2P in the high-resolution transmission electron microscopy (HRTEM) images. The high-resolution images showed lattice fringes having spacings of 2.03, 2.16 and 2.21 Å, which are assigned to the crystallographic planes of Ni (111), Ni_{12}P_5 (400) and Ni_2P (111), respectively. The observed d-spacings are consistent with the previous reports on the Ni/ Al_2O_3 [49] and $\text{Ni}_2\text{P}/\text{SiO}_2$ catalysts [50].

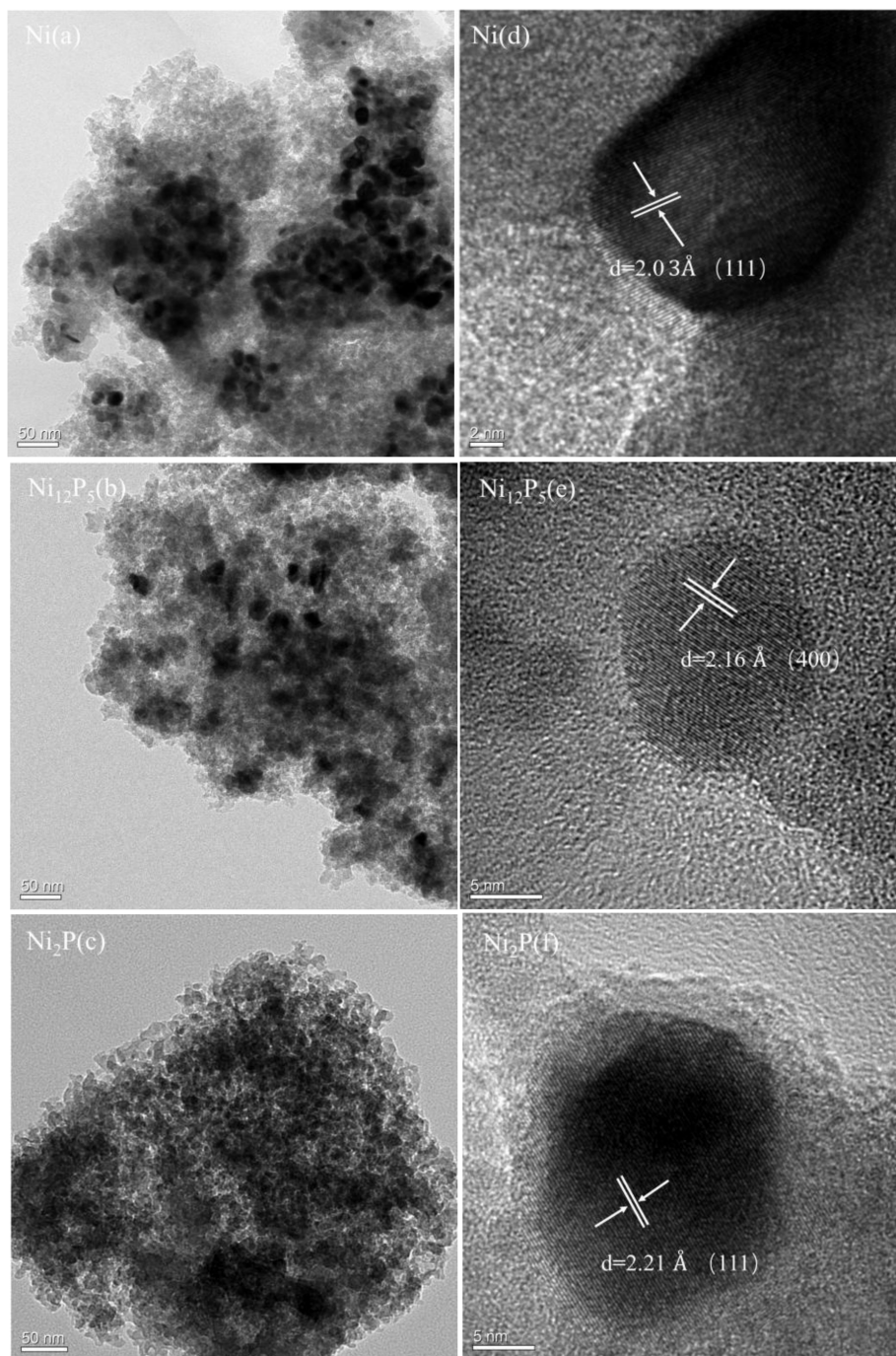


Figure 4. Transmission electron microscopy (TEM) and high-resolution TEM (HRTEM) images of the Ni/ SiO_2 (a,d), $\text{Ni}_{12}\text{P}_5/\text{SiO}_2$ (b,e) and $\text{Ni}_2\text{P}/\text{SiO}_2$ (c,f) catalysts.

2.1.6. Infrared Spectroscopy of Pyridine Adsorption (Py-IR)

The surface acidity of the phosphide catalysts were determined by infrared spectroscopy of pyridine adsorption. The infrared spectra in the region of $1700\sim 1400\text{ cm}^{-1}$ are shown in Figure 5.

According to the literatures [30,51], the bands at about 1446, 1490, 1577 and 1607 cm^{-1} were attributed to the vibrations of pyridine adsorbed on Lewis acid sites, and the bands at about 1544 and 1638 cm^{-1} corresponded to the vibrations of pyridine adsorbed on Brönsted acid sites. In addition, the band at 1595 cm^{-1} was ascribed to the vibration of hydrogen-bonded pyridine [52]. For the Ni/SiO₂ catalyst, the adsorption of pyridine gave rise to the bands at about 1446, 1490, 1577 and 1607 cm^{-1} attributed to Lewis acidity, which was in agreement with the literature [30]. Meanwhile it was found that only Lewis acidity existed on the Ni₁₂P₅/SiO₂ catalyst, as shown in Figure 5 [48]. In contrast, both Lewis acidity (1446, 1490, 1577 and 1607 cm^{-1}) and Brönsted acidity (1544 cm^{-1} and 1638 cm^{-1}) were observed on the Ni₂P/SiO₂ catalyst. Furthermore, the band at 1446 cm^{-1} was stronger than that at 1544 cm^{-1} , indicating the amount of Lewis acidic sites were larger than that of Brönsted acidic sites.

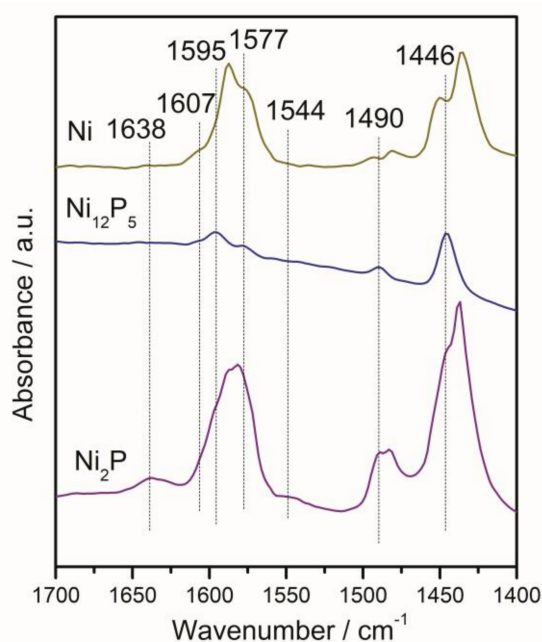


Figure 5. Infrared spectroscopy of pyridine adsorption (Py-IR) profiles of Ni/SiO₂, Ni₁₂P₅/SiO₂ and Ni₂P/SiO₂ catalysts.

2.2. The Conversion of the Palmitic Acid on the Ni/SiO₂, Ni₁₂P₅/SiO₂ and Ni₂P/SiO₂ Catalysts

The catalytic activity of the SiO₂ support, the Ni/SiO₂, Ni₁₂P₅/SiO₂ and Ni₂P/SiO₂ catalysts were evaluated in the deoxygenation reaction of palmitic acid in heptane. The gas chromatograph (GC) of products, and the activity results of the SiO₂ support and the above catalysts are shown in Figures 6 and 7, respectively. As indicated in Figure 6, only the chromatograph peak of palmitic acid was observed on SiO₂ support, showing that the palmitic acid could not be converted into hydrocarbons on SiO₂ support, which suggested that the SiO₂ support was inert for the palmitic acid conversion. On the Ni₂P/SiO₂ catalyst, palmitic acid could be partly converted into hydrocarbons, whereas palmitic acid could be completely converted into hydrocarbons and other products on the Ni/SiO₂ and Ni₁₂P₅/SiO₂ catalysts. To explore the deoxygenation pathway of palmitic acid over different catalysts, the evolution of several main products over palmitic acid conversion was plotted as a function of time in Figure 7. On the Ni/SiO₂ catalyst, the highest yield to C15 (about 69.1%) was obtained, as shown in Figure 7a, while the yield of lighter alkane C12–C14 hydrocarbons increased with reaction time and finally reached 16.2%. Furthermore, the conversion of palmitic acid on Ni/SiO₂ produced about 13.3% other substances, mainly including alkanes of less than 12 carbon atoms, and no branched paraffin was produced. The yield of C16 hydrocarbons was only about 1.4%, which indicated that C16 was the minor side product. The above results displayed that Ni/SiO₂ was favorable for the

cracking reaction and CLR [30]. During the first 2 h of reaction, a trace amount of hexadecanol was observed, which then decreased to zero after 2 h reaction. This result was in good agreement with the literature [25]. Figure 7b showed the selectivity of C15 was about 78.6% at the first hour of reaction, and then it slightly decreased to 71.1% with prolonged reaction time. The selectivity of C12–C14 slightly increased during the reaction and finally reached 27.3%. It is worth noting that the selectivity of C16 and hexadecanol were very low. The gas phase products were collected and analyzed by GC to provide additional information on the reaction. The major gas products were CH₄, C₂H₆, C₃H₈, C₄H₁₀ and CO₂, whereas CO was not observed. The quantity of CH₄ was the largest among the gas products. The CH₄ formation might be caused by methanation of CO₂ occurring ($\text{CO}_2 + 3\text{H}_2 \rightleftharpoons \text{CH}_4 + \text{H}_2\text{O}$) on the Ni/SiO₂ catalyst [15]. Thus, we speculated that DCO₂ was the main palmitic acid conversion pathway, since CO₂ could still be observed in the gas products.

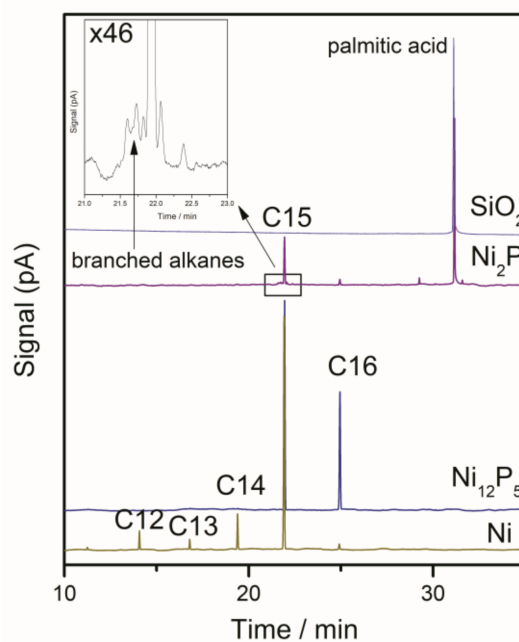


Figure 6. Gas chromatographs (GC) of the products over different samples.

For the Ni₁₂P₅/SiO₂ catalyst, the catalytic performance is given in Figure 7c,d. The palmitic acid conversion reached 100% after 6 h, and the main products were C15 and C16 hydrocarbons with about 59.8% yield for C15, and about 33.7% yield for C16. That is to say, the C15 yield was about twofold that of the C16 yield after the reaction finished. Besides, 0.5% C12–C14 hydrocarbons and about 5.8% other products were also detected, while only a small amount of hexadecanol was observed, and no branched paraffin was produced. The selectivity of C15 was maintained at about 60% during the reaction, while the C16 selectivity increased from 15.1% to 37.2%. It was noticed that the selectivity of C12–C14 and hexadecanol were very low, as shown in Figure 7d. The major component of gas products was CO accompanied by a small amount of CH₄, C₂H₆ and C₃H₈. However, CO₂ was not observed in the gas products. The above product distribution suggested that the main conversion ways of palmitic acid were the HDO and CLR reactions. However, the competition reactions for the C16 and C15 formation existed; that is, there would be two deoxygenation routes. Based on the above results, we could speculate that the main deoxygenation routes of palmitic acid were the DCO and HDO pathways with the intermediate hexadecanol.

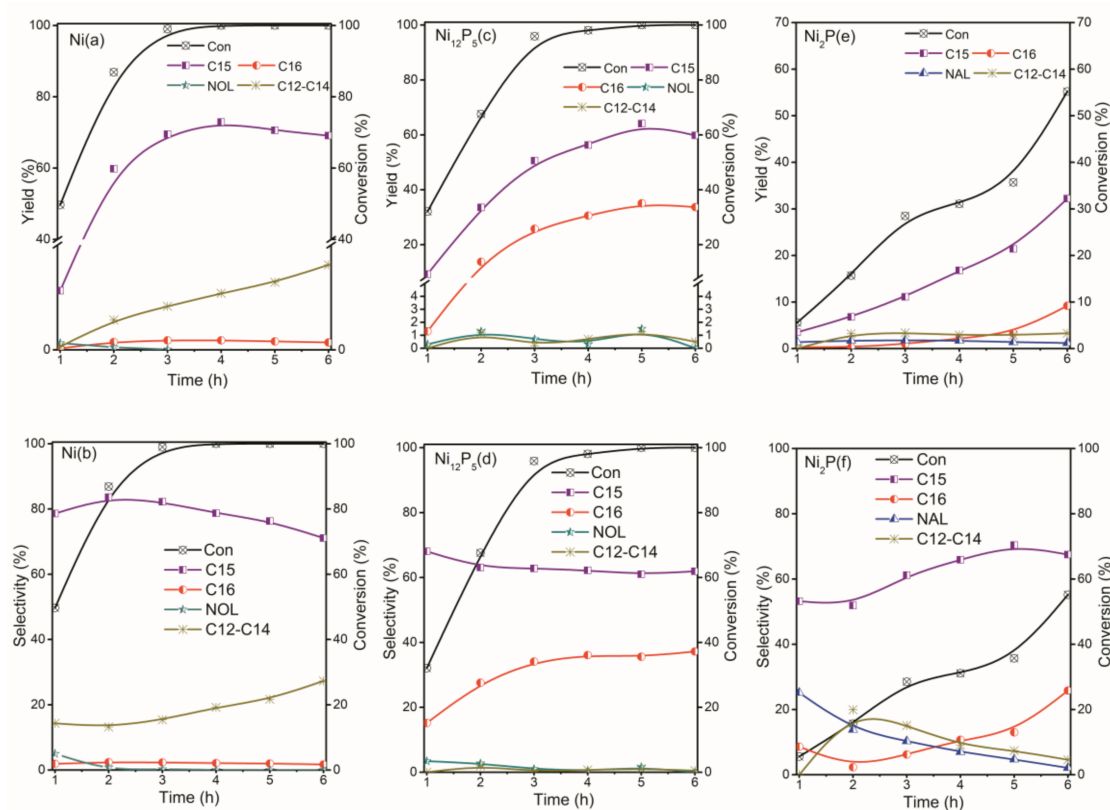


Figure 7. The conversion of palmitic acid in terms of the yields and selectivity of several typical products on the Ni/SiO₂ (a,b); Ni₁₂P₅/SiO₂ (c,d); and Ni₂P/SiO₂ (e,f) catalysts. Reaction conditions: batch reactor, 543 K, H₂ initial pressure: 1.2 MPa; stirring at 600 rpm, heptane (100 mL), catalyst (5 g L⁻¹); palmitic acid (10 g L⁻¹); NOL: hexadecanol, NAL: hexadecanal.

In contrast, the conversion of palmitic acid on Ni₂P/SiO₂ was low (about 55.2%), and the main products were hydrocarbons with 32.2% C15, 9.2% C16 and 1.8% C12-C14 as well as a small amount of branched alkanes, as shown in Figure 7e. During the palmitic acid conversion process, a small amount of hexadecanal was observed, whereas hexadecanol was not found. The selectivity of C15 increased from 53.2% to 62.7% and the selectivity of C16 increased from 8.6% to 25.8%, whereas the selectivity of C12-C14 first increased and then decreased to 4.6%; however, the selectivity of hexadecanal decreased monotonically with time, as shown in Figure 7f. The major gas product was CO accompanied by a small amount of CH₄ and C₂H₆, while CO₂ could not be observed. The above product distribution disclosed that the catalytic performance of Ni₂P/SiO₂ was poor compared to Ni/SiO₂ and Ni₁₂P₅/SiO₂. The main deoxygenation pathway of palmitic acid might be CLR reactions. The yield of C16 (9.2%) over Ni₂P/SiO₂ was less than that of C16 (33.7%) over Ni₁₂P₅/SiO₂ and much more than that of C16 (1.4%) over Ni/SiO₂, which suggested that the HDO route was following the sequence of Ni₁₂P₅/SiO₂ > Ni₂P/SiO₂ > Ni/SiO₂. The Brönsted acid sites on the Ni₂P/SiO₂ catalyst might be responsible for the formation of branched alkanes under such reaction conditions and Lewis acid sites were beneficial to the hydrocracking reaction [48].

The distinct product distributions implied the different catalytic mechanisms of the deoxygenation reactions. The different Ni species would induce different deoxygenation ways. Combined with the TOF results in Table 2, it was found that the TOF followed the sequence of Ni₁₂P₅ > Ni > Ni₂P. The high TOF on Ni₁₂P₅/SiO₂ depended on the high-index facets of Ni₁₂P₅ and the higher metal dispersion. The Lewis acid sites that existed on the three catalysts contributed to the formation of the CLR reaction products, while the Brönsted acid sites that existed on Ni₂P/SiO₂ were beneficial to the formation of the isomerization products.

2.3. The Conversion of Intermediate Hexadecanol and Hexadecanal on the Ni/SiO₂, Ni₁₂P₅/SiO₂ and Ni₂P/SiO₂ Catalysts

To further explore the deoxygenation mechanism of palmitic acid, control experiments using the feasible intermediate products, that is, hexadecanol and hexadecanal, as the reactants were carried out. The initial reaction rate based on palmitic acid conversion was obtained from the above activity data and compared with those of hexadecanal and hexadecanol conversion.

For the Ni/SiO₂ catalyst, the initial hexadecanal consumption rate (6.2 mmol·g⁻¹·h⁻¹) was higher than that of both palmitic acid (4.0 mmol·g⁻¹·h⁻¹) and hexadecanol (4.5 mmol·g⁻¹·h⁻¹), as shown in Table 4. The distribution of hydrocarbons using sole hexadecanal, or hexadecanol, as well as the 1:1 ratio mixture of hexadecanal and hexadecanol as reactants, is shown in Figure 8.

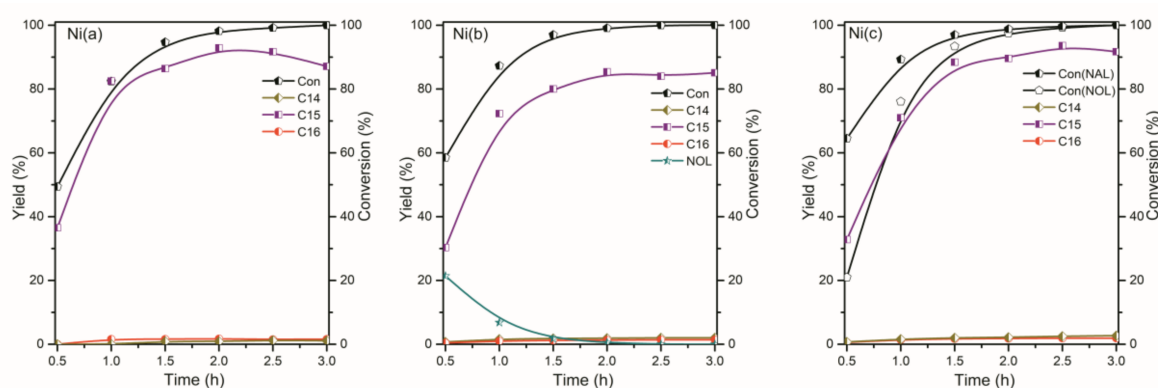


Figure 8. The conversion of reactant ((a): hexadecanol, (b): hexadecanal, (c): the ratio hexadecanal/hexadecanol = 1) and the yields of the main products as a function of reaction time on the Ni/SiO₂ catalyst. Reaction conditions: batch reactor, 543 K, H₂ initial pressure: 1.2 MPa; stirring at 600 rpm, heptane (100 mL), catalyst (5 g·L⁻¹); hexadecanal (10 g·L⁻¹), hexadecanol (10 g·L⁻¹), hexadecanal/hexadecanol = 1 (5 g·L⁻¹); NOL: hexadecanol, NAL: hexadecanal.

Table 4. The initial rate of palmitic acid consumption and the hydrogenation rate of hexadecanal and hexadecanol over Ni/SiO₂, Ni₁₂P₅/SiO₂ and Ni₂P/SiO₂ (mmol·g⁻¹·h⁻¹).

Catalyst	Palmitic Acid	Hexadecanal	Hexadecanol
Ni	4.0	6.2	4.5
Ni ₁₂ P ₅	2.6	4.1	3.7
Ni ₂ P	0.2	1.9	1.9

The hexadecanol conversion over the Ni/SiO₂ catalyst is shown in Figure 8a; the hexadecanol conversion in the presence of H₂ yielded mainly C15 accompanied by trace amounts of C14 and C16; the gas products were CH₄ accompanying with a trace amount of C₂H₆; however, CO and CO₂ were not observed. Peng et al. reported that C–C bond cleavage for alcohols with terminal hydroxyl groups occurred via DCO of aldehydes (generated by dehydrogenation of alcohols) over Pt/Al₂O₃ catalysts [53,54], so we considered that the hexadecanol was mainly converted into C15 hydrocarbon via the route of DCO over the Ni/SiO₂ catalyst, and CH₄ might be formed via the methanation of CO. As can be seen from Figure 8b, the hexadecanal conversion also yielded mainly C15 accompanied by trace amounts of C14 and C16, and the C15 yield obviously increased in the first 1.5 h; hexadecanol was also observed, and its yield decreased quickly from 20% to 0.5% within 2 h, and then became zero with the reaction time extending. Obviously, the sum amount of C15 and the intermediate hexadecanol yield was approximately equal to the conversion of hexadecanal, which suggested that the conversion of hexadecanal might proceed via the intermediate hexadecanol, which then formed the C15 by DCO on the Ni/SiO₂ catalyst. The trace amount of C16 was from the dehydration of the

intermediate hexadecanol, since there was also a trace amount of C16 formation in the separated study using hexadecanol as reactant. The only gas product was CH₄; while CO and CO₂ were not observed, therefore the CH₄ formation might be caused by the methanation of CO. The results demonstrated that the product distribution from hexadecanal was similar to that from hexadecanol. As shown in Figure 8c, when the hexadecanal and hexadecanol mixture in a 1:1 ratio were chosen as the reactants, it was found that the hexadecanal conversion was higher than the hexadecanol in the first 2 h and, finally, their conversion reached 100%; and the initial consumption of the hexadecanal (6.2 mmol·g⁻¹·h⁻¹) was higher than that of the hexadecanol (4.5 mmol·g⁻¹·h⁻¹), which suggested that the Ni/SiO₂ catalyst was beneficial for the hexadecanal conversion compared with the hexadecanol; the main product C15 was about 90% after the reaction finished, which also suggested that the hexadecanal and hexadecanol were mainly converted into C15 accompanied by CO released via DCO; the gas CO was converted into CH₄ by the methanation reaction, consistent with the results of the separate study of sole hexadecanal or hexadecanol.

Nevertheless, we found that C15 was the main product accompanied by trace amounts of C12-C14 and C16 all the time of the reaction process when palmitic acid was used as reactant, as shown in Figure 7. It was interesting that the palmitic acid conversion tendency was the same as the yield of C15. Furthermore, the ratio of the main products, C15/C16, from the palmitic acid, hexadecanal, hexadecanal and hexadecanal/hexadecanol (1:1 weight ratio) conversion are shown in Figure 9. It can be observed that the amount of C15 was much higher than that of C16, varying from 45- to 70-fold, while the C15/C16 ratio from palmitic acid conversion was the lowest among those reactions. If the palmitic acid conversion into alkanes via hexadecanal and/or hexadecanol were the main deoxygenation pathway on Ni/SiO₂, we would get a higher C15/C16 ratio of hydrocarbons. However, the C15/C16 ratio was the lowest among the reactions using different starting materials. Therefore, we reasonably speculated that there was another reaction route for the formation of C15. Combined with the gas products from hexadecanal and hexadecanol conversion, CH₄ was main gas product and might be from CO by methanation [3], whereas the main gas products from palmitic acid conversion were CH₄, C₂H₆ and CO₂. So, we can conclude that the formation of C15 might be from the C-C cleavage of palmitic acid accompanying the CO₂ release, which was the main deoxygenation route for the palmitic acid conversion into hydrocarbon over the Ni/SiO₂ catalyst. Furthermore, the trace amount of intermediate hexadecanol was detected in the first 2 h of palmitic acid conversion on Ni/SiO₂, which finally converted into C15 by DCO. Because the hexadecanol was almost completely converted into C15 according to the above results, there was a minor deoxygenation route via the intermediate hexadecanol, most of which converted into C15 via DCO, while the remaining hexadecanol produced the trace amount of C16 via HDO. Consequently, we can conclude that the main deoxygenation pathways of palmitic acid on the Ni/SiO₂ catalyst were the C-C cleavage via DCO₂ with minor intermediate hexadecanol formation, and then the hexadecanol further converted into alkane via DCO and HDO.

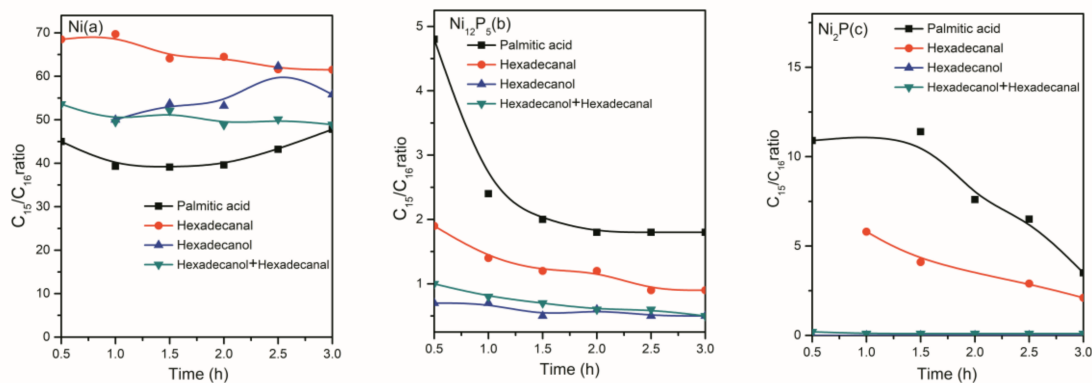


Figure 9. The ratio of C15/C16 hydrocarbons over the Ni/SiO₂ (a); Ni₁₂P₅/SiO₂ (b) and Ni₂P/SiO₂ (c) catalysts.

On the $\text{Ni}_{12}\text{P}_5/\text{SiO}_2$ catalyst, the initial rate of palmitic acid consumption ($2.6 \text{ mmol}\cdot\text{g}^{-1}\cdot\text{h}^{-1}$) was less than that of the hexadecanal ($4.1 \text{ mmol}\cdot\text{g}^{-1}\cdot\text{h}^{-1}$) and the hexadecanol ($3.7 \text{ mmol}\cdot\text{g}^{-1}\cdot\text{h}^{-1}$). The hexadecanol conversion over $\text{Ni}_{12}\text{P}_5/\text{SiO}_2$ catalyst is shown in Figure 10a. The conversion of hexadecanol yielded C15 and C16, while the C16 yield was much higher than that of the C15 yield after the reaction finished, and the gas products were also mainly CO accompanied by a small amount of CH_4 and C_2H_6 . The C16 was formed by the hexadecanol conversion via HDO, whereas the C15 was formed by the hexadecanol conversion via DCO, which suggested that the hexadecanol conversion over the $\text{Ni}_{12}\text{P}_5/\text{SiO}_2$ catalyst was mainly through the HDO route. The conversion of hexadecanal yielded C15 and C16 accompanying the hexadecanol formation, and the C15 yield was slightly higher than that of C16 within the 2.5 h reaction, as shown in Figure 10b, whereas the amount of hexadecanol increased first and then decreased; but the C16 yield was finally slightly higher than that of C15 after the reaction finished, and the gas products were mainly CO accompanied by a small amount of CH_4 and C_2H_6 , which suggested that the hexadecanal conversion over the $\text{Ni}_{12}\text{P}_5/\text{SiO}_2$ catalyst was via both HDO and direct DCO. At the beginning of the reaction, the direct DCO was the main deoxygenation route because the amount of C15 was higher than that of C16. Prolonging the reaction time, the amount of C16 increased fast since the intermediate hexadecanol converted into C16 via HDO, which was consistent with the above results of the hexadecanol conversion. So, we can conclude that the hexadecanal conversion was through two routes over the $\text{Ni}_{12}\text{P}_5/\text{SiO}_2$ catalyst, that is, the HDO and direct DCO of hexadecanal, which proceeded competitively.

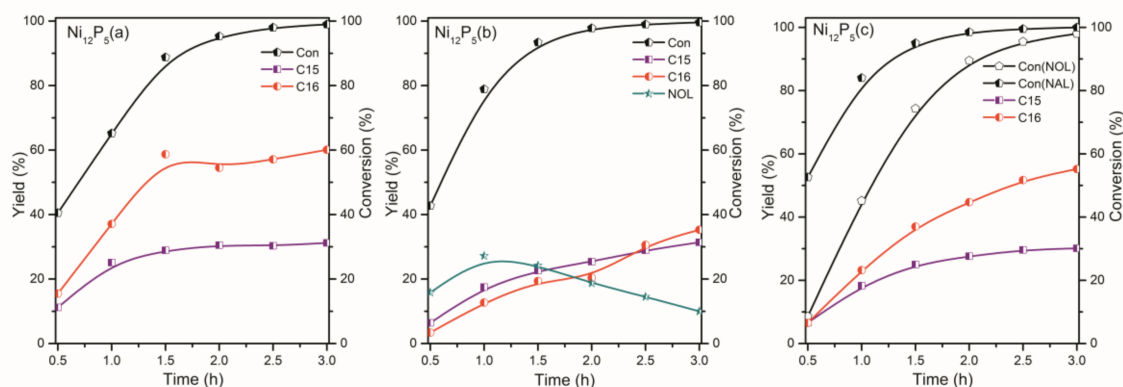


Figure 10. The conversion of reactant ((a): hexadecanol, (b): hexadecanal, (c): the ratio hexadecanal/hexadecanol = 1) and the yields of the main products as a function of reaction time on the $\text{Ni}_{12}\text{P}_5/\text{SiO}_2$ catalyst. Reaction conditions: batch reactor, 543 K, H_2 initial pressure: 1.2 MPa; stirring at 600 rpm, heptane (100 mL), catalyst ($5 \text{ g}\cdot\text{L}^{-1}$); hexadecanal ($10 \text{ g}\cdot\text{L}^{-1}$), hexadecanol ($10 \text{ g}\cdot\text{L}^{-1}$), hexadecanal/hexadecanol = 1 ($5 \text{ g}\cdot\text{L}^{-1}$); NOL: hexadecanol, NAL: hexadecanal.

When the hexadecanal and hexadecanol mixture of 1:1 ratio were chosen as the reactants, as shown in Figure 10c, it was found that the hexadecanal conversion was higher than the hexadecanol, which also suggested that the $\text{Ni}_{12}\text{P}_5/\text{SiO}_2$ catalyst was beneficial for the hexadecanal conversion compared with the hexadecanol, which agreed with the fact that the consumption rate of hexadecanal ($4.1 \text{ mmol}\cdot\text{g}^{-1}\cdot\text{h}^{-1}$) was slightly higher than that of the hexadecanol ($3.7 \text{ mmol}\cdot\text{g}^{-1}\cdot\text{h}^{-1}$). The C16 yield was higher than that of C15 after the reaction finished, which was caused by the fact that the main product was both C16 in the separate study of sole hexadecanal or hexadecanol. The gas products from hexadecanal and hexadecanol conversion were mainly CH_4 and CO, while the main gas products from palmitic acid conversion were mainly CH_4 , C_2H_6 and CO. Furthermore, the separate study of the intermediate hexadecanal showed that the amount of C15 was slightly less than that of C16, and the separate study of hexadecanol discovered that the amount of C15 was half of that of C16. In fact, the C15/C16 ratio was approximately twofold during the palmitic acid conversion process, which implied that the main route of C15 formation might be from the C–C cleavage via

DCO of palmitic acid. Besides, the C15/C16 ratio of hydrocarbons from the palmitic acid conversion was the highest among all the reactions on $\text{Ni}_{12}\text{P}_5/\text{SiO}_2$, as shown in Figure 9. If the palmitic acid conversion into alkanes via hexadecanal and/or hexadecanol were the main deoxygenation pathway on $\text{Ni}_{12}\text{P}_5/\text{SiO}_2$, we would get the lower C15/C16 ratio of hydrocarbons. Accordingly, there was still a C–C cleavage of palmitic acid accompanying the CO and H_2O release. On the other hand, hexadecanol was observed, while hexadecanal could not be detected during the palmitic acid conversion on $\text{Ni}_{12}\text{P}_5/\text{SiO}_2$, which could be accounted for by the consumption rate of hexadecanal being faster than that of hexadecanol. Therefore, for the $\text{Ni}_{12}\text{P}_5/\text{SiO}_2$ catalyst, we can confirm that there were two main deoxygenation pathways of palmitic acid: one pathway was the C–C cleavage via direct DCO of palmitic acid to form C15 alkane; and the other pathway was HDO of palmitic acid directly generating hexadecanol; the subsequent dehydration of hexadecanol yielded C16 hydrocarbon via HDO, and those two routes proceeded competitively over the $\text{Ni}_{12}\text{P}_5/\text{SiO}_2$ catalyst.

For the $\text{Ni}_2\text{P}/\text{SiO}_2$ catalyst, the initial consumption rate of hexadecanal and hexadecanol were both $1.9 \text{ mmol}\cdot\text{g}^{-1}\cdot\text{h}^{-1}$. The hexadecanol conversion on $\text{Ni}_2\text{P}/\text{SiO}_2$ resulted in C16 alkane accounting for approximately 80% of the products, whereas the C15 alkane was observed as a minor product as shown in Figure 11a. The gas products were also mainly CH_4 and C_2H_6 , which suggested that the conversion of hexadecanol was mainly through the route of HDO on the $\text{Ni}_2\text{P}/\text{SiO}_2$ catalyst. The hexadecanal conversion was lower, as seen in Figure 11b. The C15 yield was higher than that of C16, and hexadecanol was also obviously observed. The gas products were mainly CH_4 and C_2H_6 , while the CH_4 formation might be caused by methanation of CO. From the above results, we can conclude that the hexadecanal conversion was mainly through the direct DCO pathway, while the HDO route via the intermediate hexadecanol also existed, which seemed to be the subordinate deoxygenation route. When the hexadecanal and hexadecanol mixture of 1:1 ratio were chosen as the reactants, the hexadecanol conversion was higher than that of the hexadecanal conversion, as shown in Figure 11c. The main product was C16. The intermediate hexadecanol could not be completely converted after 3 hours' reaction in the separate study of hexadecanal, and the product was mainly C16 in the separate study solely of hexadecanol. The gas products were detected from the separate study of hexadecanal and it was found that CH_4 was the main gas product; which might be from CO transformation by the methanation reaction [3]. The C15/C16 ratio of hydrocarbons from the palmitic acid conversion was the highest among the reactions using different starting materials on $\text{Ni}_2\text{P}/\text{SiO}_2$, as shown in Figure 9. If the palmitic acid conversion into alkanes via hexadecanal and/or hexadecanol were the main deoxygenation pathways on $\text{Ni}_2\text{P}/\text{SiO}_2$, we would get a low C15/C16 ratio of hydrocarbons. This tendency was similar to that of the $\text{Ni}_{12}\text{P}_5/\text{SiO}_2$ catalyst. Accordingly, there was still a C–C cleavage of palmitic acid accompanying the CO and H_2O release. Combined with the above results, we inferred that the C–C cleavage of palmitic acid could also occur on $\text{Ni}_2\text{P}/\text{SiO}_2$. On the other hand, the intermediate hexadecanal was observed in the palmitic acid conversion experiment. Thus, combined with the gas and liquid products, we can conclude that there were two main deoxygenation pathways of palmitic acid on the $\text{Ni}_2\text{P}/\text{SiO}_2$ catalyst: one pathway was the C–C cleavage of palmitic acid via DCO to form C15 alkane; and the other pathway was HDO of palmitic acid to generate hexadecanal, which subsequently directly released CO to form C15 alkane. Based on a little amount of C16 alkane formed, we speculated that a side reaction was the palmitic acid conversion into C16 alkane by the HDO pathway.

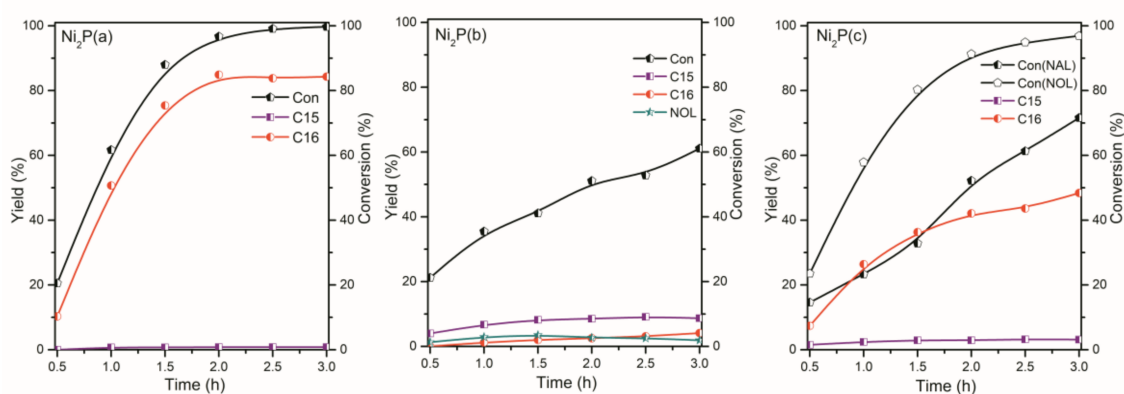


Figure 11. The conversion of reactant ((a): hexadecanal, (b): hexadecanal, (c): the ratio hexadecanal/hexadecanal = 1) and the yields of the main products as a function of reaction time on the Ni₂P/SiO₂ catalyst. Reaction conditions: batch reactor, 543 K, H₂ initial pressure: 1.2 MPa; stirring at 600 rpm, heptane (100 mL), catalyst (5 g·L⁻¹); hexadecanal (10 g·L⁻¹), hexadecanal (10 g·L⁻¹), hexadecanal/hexadecanal = 1 (5 g·L⁻¹); NOL: hexadecanal, NAL: hexadecanal.

2.4. The Kinetic Parameters

The rate constants for the consumption of palmitic acid, hexadecanal and hexadecanol on the Ni/SiO₂, Ni₁₂P₅/SiO₂ and Ni₂P/SiO₂ catalysts are summarized in Table 5. According to previous reports [55,56], the deoxygenation of palmitic acid, hexadecanal and hexadecanol were considered a first order reaction. The obtained rate constants are not very sensitive to reaction materials on the Ni/SiO₂ and Ni₁₂P₅/SiO₂ catalysts. The fact that $k(\text{palmitic acid}) > k(\text{hexadecanal}) \approx k(\text{hexadecanol})$ suggested that the palmitic acid conversion was faster than hexadecanal and hexadecanol on Ni/SiO₂ and Ni₁₂P₅/SiO₂. Hexadecanol was detected during the palmitic acid conversion progress, while hexadecanal was not observed on the Ni/SiO₂ and Ni₁₂P₅/SiO₂ catalysts. In addition, the rate constant of hexadecanal conversion (k) to products was equal to that of hexadecanol conversion (k), which was perhaps why only hexadecanol was observed as the intermediate product on Ni₁₂P₅/SiO₂ during the palmitic acid conversion. On the contrary, the fact that $k(\text{palmitic acid}) \approx k(\text{hexadecanal}) < k(\text{hexadecanol})$ on the Ni₂P/SiO₂ catalyst suggested that the conversion of palmitic acid and hexadecanal were lower than that of hexadecanol. Furthermore, hexadecanal was detected during the palmitic acid conversion. So, the hydrogenation of palmitic acid to hexadecanal was prevalent, relative to other parallel reactions of the C–C cleavage via DCO and HDO. The extremely low rate constants of palmitic acid and hexadecanal on Ni₂P/SiO₂ demonstrate the poor catalytic performance of palmitic acid and hexadecanal conversion.

Table 5. The kinetic data of the Ni/SiO₂, Ni₁₂P₅/SiO₂ and Ni₂P/SiO₂ catalysts.

Catalyst	k (h ⁻¹)			Ea (kJ/mol)	A (h ⁻¹)
	Palmitic Acid	Hexadecanal	Hexadecanol		
Ni/SiO ₂	1.50	1.02	1.02	85	4.5 × 10 ⁸
Ni ₁₂ P ₅ /SiO ₂	1.08	0.81	0.80	93	8.4 × 10 ⁸
Ni ₂ P/SiO ₂	0.11	0.14	1.03	51	3.0 × 10 ³

According to the kinetic experiments, the apparent activation energy of and pre-exponential factor for the palmitic acid conversion were obtained and are listed in Table 5. The activation energy followed the sequence: $E_a(\text{Ni}_2\text{P}/\text{SiO}_2) < E_a(\text{Ni}/\text{SiO}_2) < E_a(\text{Ni}_{12}\text{P}_5/\text{SiO}_2)$, it was apparent that the pre-exponential factor followed the same sequence. However, the activity experiments results from TOF disclosed that Ni₁₂P₅/SiO₂ was exhibited excellently, while Ni₂P/SiO₂ displayed a poor

performance. Furthermore, the catalyst Ni_{12}P_5 index facet was (400) according to the HRTEM results. We speculated that the high-index facets might influence for the catalysis activity for the conversion of palmitic acid. Combined with the above results, we concluded that the excellent catalytic performance of $\text{Ni}_{12}\text{P}_5/\text{SiO}_2$ was ascribed to high-index facets, high metal dispersion and high pre-exponential, whereas the poor catalytic performance of $\text{Ni}_2\text{P}/\text{SiO}_2$ was attributed to poor metal dispersion and the big crystallite size.

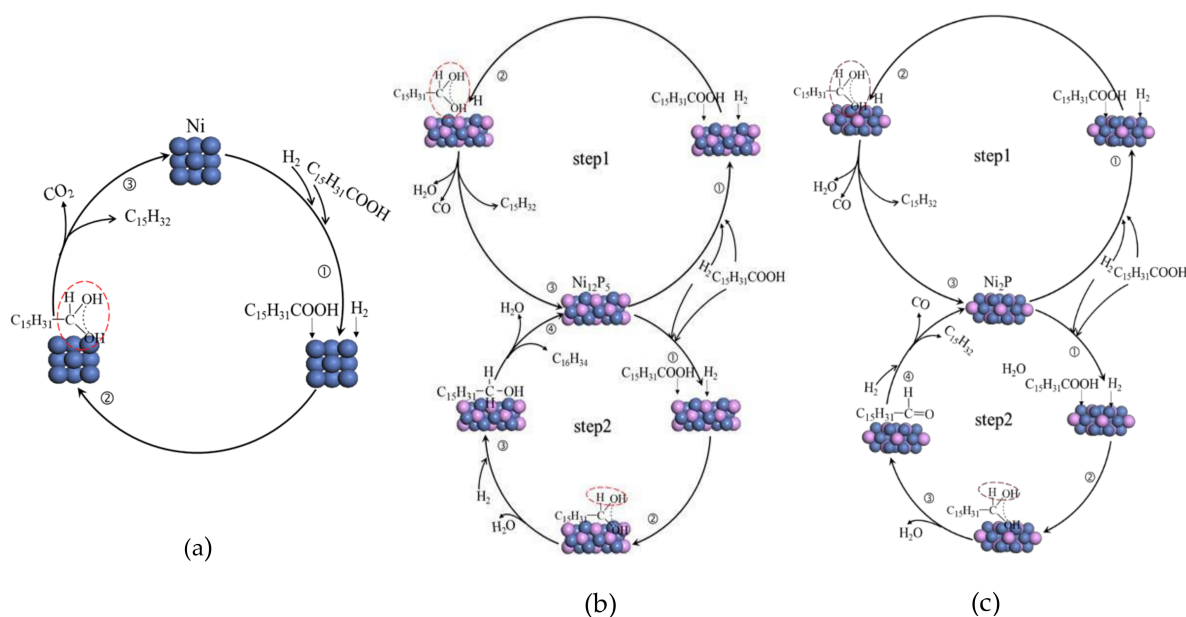
2.5. Summary of Reaction Pathway

Combination of the reaction of palmitic acid, hexadecanal and hexadecanol allowed us to formulate the overall reaction pathways for the conversion of palmitic acid on the Ni/SiO_2 , $\text{Ni}_{12}\text{P}_5/\text{SiO}_2$ and $\text{Ni}_2\text{P}/\text{SiO}_2$.

The process of the main deoxygenation pathways of palmitic acid on the Ni/SiO_2 catalyst was the C–C cleavage to form the main product of C15 and CO_2 in Scheme 2a [19]. Another side reaction was palmitic acid converted into hexadecanol via HDO. After the formation of hexadecanol, two parallel reactions occurred, that is, the majority of hexadecanol was converted into C15 via DCO and a small amount of hexadecanol was converted into C16 by HDO catalyzed by metallic Ni sites.

The $\text{Ni}_{12}\text{P}_5/\text{SiO}_2$ catalyst has DCO and HDO activity at 543 K under H_2 . Therefore, we can confirm that there were two main competition deoxygenation pathways of palmitic acid on the $\text{Ni}_{12}\text{P}_5/\text{SiO}_2$ catalyst. One pathway was the C–C cleavage via DCO of palmitic acid to form C15 alkanes (Step 1, Scheme 2b), and the other pathway was HDO of palmitic acid to generate hexadecanol as the intermediate, and then the hexadecanol converted into C16 via hydrodeoxygenation. Furthermore, C16 selectivity was higher compared with other reactions. Apparently, hexadecanol via HDO was favored for C16 formation over $\text{Ni}_{12}\text{P}_5/\text{SiO}_2$.

On $\text{Ni}_2\text{P}/\text{SiO}_2$, the palmitic acid conversion had two main reaction pathways. One pathway was the direct C–C cleavage via DCO of the palmitic acid to form C15 alkane (Step 1, Scheme 2c), and the other pathway was that palmitic acid was firstly converted into hexadecanal, and then hexadecanal released CO to form C15 (Step 2, Scheme 2c). In addition, the hexadecanal of HDO was inhibited and C16 selectivity was markedly low.



Scheme 2. (a) The suggested main reaction pathways of palmitic acid over the Ni/SiO_2 catalyst; (b) the suggested main reaction pathways of palmitic acid over the $\text{Ni}_{12}\text{P}_5/\text{SiO}_2$ catalyst; (c) the suggested main reaction pathways of palmitic acid over the $\text{Ni}_2\text{P}/\text{SiO}_2$ catalyst.

3. Experiment

3.1. Catalyst Synthesis

The Ni/SiO₂, Ni₁₂P₅/SiO₂ and Ni₂P/SiO₂ catalysts were synthesized by incipient wetness impregnation followed by temperature programmed reduction (TPR). The controlled Ni content calculated using Equation (1) for all catalysts was 24.20 wt %, and the content of P was adjusted by the molar ratios of Ni/P. The controlled Ni/P molar ratios of 0.5/1 and 1.5/1 led to the formation of Ni₂P and Ni₁₂P₅ catalysts, respectively. Before impregnation, the silica support was sieved to 40–60 mesh and dried at 873 K for 4 h in ambient air. The dried silica support was first impregnated with a mixture aqueous solution of Ni(NO₃)₂•6H₂O and NH₄H₂PO₄ or only Ni(NO₃)₂•6H₂O, followed by ultrasonic treatment for 4 h, and the impregnation lasted for 24 h. Then, the catalyst precursor was dried in an oil bath at 353 K, and followed by drying at 383 K overnight and calcination at 873 K for 4 h in ambient air. Thereafter, the precursor sample was reduced from room temperature to 873 K at a rate of 2 K·min⁻¹ and maintained at 873K for 2 h under flowing H₂ (99.999%, 30 mL·min⁻¹), and then cooled to room temperature under flowing N₂ to obtain the active nickel phosphide catalysts and Ni catalyst.

$$\text{wt \% Ni} = [\text{weight of Ni}/(\text{weight of Ni} + \text{weight of SiO}_2)] \times 100\% \quad (1)$$

3.2. Catalyst Characterization

The BET specific surface area was determined by nitrogen adsorption–desorption at 77 K using a Micromeritics Tristar II 3020 instrument. Before measurement, the samples were activated in vacuum at 393 K and 573 K for 2 h respectively. The pore volumes and average pore diameters were determined by the Barrett–Joyner–Halenda (BJH) method from the desorption branches of the isotherms.

XRD patterns were recorded using a SHIMADZU XRD-6100 diffractometer equipped with Cu-Kα monochromatized radiation generated at 40 kV and 30 mA. Powder diffraction patterns were recorded over the 2θ range of 30–80° at a scan rate of 1°·min⁻¹.

XPS experiments were performed on an AXIS Ultra DLD (KRATOS) spectrometer using a pass energy of 50 eV (0.1 eV per step) with a monochromatic Al-Kα X-ray source. Binding energy (BE) of various elements have been referenced to the C1s at 284.6 eV. A Shirley background was subtracted from all spectra and peak fitting was performed using an 80/20 Lorentz–Gauss function.

The actual Ni and P loadings were determined by atomic absorption spectroscopy using a VG PQExCell. Prior to measurement, the samples were dissolved in a mixture of hydrofluoric acid (48%) and nitric acid.

TEM images of the samples were obtained on an FEI Tecnai G2 20 TWIN instrument at an acceleration voltage of 200 kV.

Hydrogen chemisorption and H₂-TPD measurements were performed using the Micromeritics Autochem II 2920 instrument. Approximately 0.1 g of catalyst was flashed firstly in a 10 mL·min⁻¹ flow of Ar at room temperature for 2 h. The catalysts were activated at 673 K in a flow of Ar and hold for 1 h at 50 mL min⁻¹, then cooled down to 273 K. The H₂ chemisorption was measured by injecting pulses of 10% vol % H₂-Ar flow (50 mL·min⁻¹) at 3 min intervals until adsorption saturation at 273 K. Next, the samples were heated from 273 K to 325 K and held for 1 h in a flow of Ar at 50 mL·min⁻¹, the temperature was then increased to 873 K at the rate of 10 K·min⁻¹ to obtain the desorption curve, and the hydrogen adsorption volume capacity, denoted as V(H₂), was obtained by manual integration of the desorption curve. The mole active sites were calculated according to Equation (2):

$$n \text{ (the mole of Ni active sites)} = 2n(\text{H}_2) = \text{PV}(\text{H}_2)/RT \quad (2)$$

A Ni atom was assumed to adsorb one H atom, therefore, the mole of Ni active sites should be equal to 2n(H₂). We have revised in the manuscript.

The acid sites of catalysts were determined by infrared (IR) spectroscopy with pyridine as probe molecule. The IR spectrum was measured with a BRUKER VERTEX 70 spectrometer with a resolution of 4 cm^{-1} (number of scans, 16). The samples were activated at 673 K for 2 h in vacuum, and a background spectrum was recorded when the temperature was decreased to 303 K. The activated samples were exposed to pyridine vapor at 303 K for 0.5 h in vacuum. After pyridine adsorption finished, the spectrum was recorded.

3.3. Measurement of Catalytic Reaction

We selected saturated palmitic acid as the model compound. The Ni/SiO₂, Ni₁₂P₅/SiO₂ and Ni₂P/SiO₂ catalysts were tested. The typical experiment was carried out as follows: palmitic acid reactant (1.0 g), heptane solvent (100 mL), and catalyst (5 g·L⁻¹) were charged into a batch autoclave (Parr Instrument, 300 mL, Moline, Illinois, USA). Before starting the reaction, N₂ was charged into the batch autoclave several times to replace air, and then pure H₂ was charged to 1.2 MPa at room temperature. The reaction was carried out at 543 K with stirring at 600 rpm for 6 h. During the reaction, the liquid products were sampled at intervals of one hour and analyzed by GC when the reaction temperature reached 543 K. The separated experiments with hexadecanal, hexadecanol as reactants were carried out respectively for 3 h under the same reaction conditions except that the liquid products were analyzed at the intervals of half an hour.

3.4. Product Analysis

The liquid products were quantitatively analyzed using a gas chromatograph (GC, PANNA A91) equipped with a HP-5 capillary column (30 m × 0.25 mm × 0.25 μm) and a flame ionization detector (FID). N₂ was used as the carrier gas. The internal standard (i.e., 2-Ethylbutyric acid) was used for quantification. Both injection and detection temperatures were 593 K. The temperature program was set as: 343 K (3 min), 5 K·min⁻¹, 433 K, 10 K·min⁻¹, 553 K (10 min). The gas products were analyzed using a gas chromatograph (GC, PANNA A91) equipped with a EC-1 (30 m × 0.53 mm × 0.5 μm) capillary column and FID, PQ column and 5A column with thermal conductivity detector (TCD). The yield (Yield) was calculated by Equation (3).

$$\text{Yield} = (W_{\text{product}}/M_{\text{product}})/(W_{\text{reactant}}/M_{\text{reactant}}) \times 100\% \quad (3)$$

where W_{product} and W_{reactant} are the weights of the product and reactant, and M_{product} and M_{reactant} are the molecular weight of the product and reactant, respectively.

4. Conclusions

Ni₁₂P₅/SiO₂ showed higher catalytic performance compared with Ni/SiO₂ and Ni₂P/SiO₂ due to its higher metal dispersion, high-index crystal and high pre-exponential. The Ni/SiO₂ and Ni₁₂P₅/SiO₂ catalysts were more favourable for the hexadecanal conversion than for hexadecanol. In contrast, Ni₂P/SiO₂ was benefited for hexadecanol conversion compared with hexadecanal. The nature of Ni-species affected the activity and reaction pathway. Ni/SiO₂ mainly catalyzed DCO₂ of palmitic acid to product diesel-range hydrocarbon (C15) accompanied with the side reaction of the C–C cleavage to produce diesel-range hydrocarbon C12–C14. Ni₁₂P₅/SiO₂ exhibits DCO and HDO activity from palmitic acid, and there are competition deoxygenation pathways. One is a direct DCO pathway to yield C15, and the other is the palmitic acid conversion via hexadecanol as the intermediate product that is then converted into C16. In contrast, the palmitic acid deoxygenation on Ni₂P/SiO₂ occurs easily via direct DCO to form C15 and HDO to the product hexadecanal, and then the hexadecanal is converted into C15 by releasing CO.

Acknowledgments: This work was financially supported by Collaborative Fund of the Ministry of Education (No. 6141A02033508), the National Natural Science Foundation of China (National Special Scientific Research Instrument and Equipment Development No. 21427803-2) and 111 project (No. B17030) and the National Natural

Science Foundation of China (No. 21303109). We would like to thank Yunfei Tian of the analytical and testing center of Sichuan University for the XPS experiments.

Author Contributions: The manuscript was written from the contributions of all the authors. Wenjun Zhou is responsible for the main experiment and partly for the writing; Hui Xin, Huiru Yang, Xiangze Du, Rui Yang for part of the experiments and analysis; Dan Li for part of the experiment, analysis, and major writing; and Changwei Hu for design and revision. All authors have given approval to the final version of the manuscript.

Conflicts of Interest: The authors declare no conflict of interest.

References

1. Ma, B.; Zhao, C. High-grade diesel production by hydrodeoxygenation of palm oil over a hierarchically structured Ni/HBEA catalyst. *Green Chem.* **2015**, *17*, 1692–1701. [[CrossRef](#)]
2. Koike, N.; Hosokai, S.; Takagaki, A.; Nishimura, S.; Kikuchi, R.; Ebitani, K.; Suzuki, Y.; Oyama, S.T. Upgrading of pyrolysis bio-oil using nickel phosphide catalysts. *J. Catal.* **2016**, *333*, 115–126. [[CrossRef](#)]
3. Pattanaik, B.P.; Misra, R.D. Effect of reaction pathway and operating parameters on the deoxygenation of vegetable oils to produce diesel range hydrocarbon fuels: A review. *Renew. Sustain. Energy Rev.* **2017**, *73*, 545–557. [[CrossRef](#)]
4. Santillan-Jimenez, E.; Morgan, T.; Lacny, J.; Mohapatra, S.; Crocker, M. Catalytic deoxygenation of triglycerides and fatty acids to hydrocarbons over carbon-supported nickel. *Fuel* **2013**, *103*, 1010–1017. [[CrossRef](#)]
5. Kim, S.K.; Han, J.Y.; Lee, H.-S.; Yum, T.; Kim, Y.; Kim, J. Production of renewable diesel via catalytic deoxygenation of natural triglycerides: Comprehensive understanding of reaction intermediates and hydrocarbons. *Appl. Energy* **2014**, *116*, 199–205. [[CrossRef](#)]
6. Liu, Y.; Yao, L.; Xin, H.; Wang, G.; Li, D.; Hu, C. The production of diesel-like hydrocarbons from palmitic acid over HZSM-22 supported nickel phosphide catalysts. *Appl. Catal. B* **2015**, *174*, 504–514. [[CrossRef](#)]
7. Moore, R.H.; Thornhill, K.L.; Weinzierl, B.; Sauer, D.; D’Ascoli, E.; Kim, J.; Lichtenstern, M.; Scheibe, M.; Beaton, B.; Beyersdorf, A.J.; et al. Biofuel blending reduces particle emissions from aircraft engines at cruise conditions. *Nature* **2017**, *543*, 411–415. [[CrossRef](#)] [[PubMed](#)]
8. Saidi, M.; Samimi, F.; Karimipourfard, D.; Nimmanwudipong, T.; Gates, B.C.; Rahimpour, M.R. Upgrading of lignin-derived bio-oils by catalytic hydrodeoxygenation. *Energy Environ. Sci.* **2014**, *7*, 103–129. [[CrossRef](#)]
9. Srifa, A.; Viriya-empikul, N.; Assabumrungrat, S.; Faungnawakij, K. Catalytic behaviors of Ni/ γ -Al₂O₃ and Co/ γ -Al₂O₃ during the hydrodeoxygenation of palm oil. *Catal. Sci. Technol.* **2015**, *5*, 3693–3705. [[CrossRef](#)]
10. Chen, J.; Xu, Q. Hydrodeoxygenation of biodiesel-related fatty acid methyl esters to diesel-range alkanes over zeolite-supported ruthenium catalysts. *Catal. Sci. Technol.* **2016**, *6*, 7239–7251. [[CrossRef](#)]
11. Xia, Q.; Zhuang, X.; Li, M.M.; Peng, Y.K.; Liu, G.; Wu, T.S.; Soo, Y.L.; Gong, X.Q.; Wang, Y.; Tsang, S.C. Cooperative catalysis for the direct hydrodeoxygenation of vegetable oils into diesel-range alkanes over Pd/NbOPO₄. *Chem. Commun.* **2016**, *52*, 5160–5163. [[CrossRef](#)] [[PubMed](#)]
12. Qin, Y.; Chen, P.; Duan, J.; Han, J.; Lou, H.; Zheng, X.; Hong, H. Carbon nanofibers supported molybdenum carbide catalysts for hydrodeoxygenation of vegetable oils. *RSC Adv.* **2013**, *3*, 17485. [[CrossRef](#)]
13. Liu, J.; Liu, C.; Zhou, G.; Shen, S.; Rong, L. Hydrotreatment of jatropha oil over NiMoLa/Al₂O₃ catalyst. *Green Chem.* **2012**, *14*, 2499. [[CrossRef](#)]
14. Han, J.; Duan, J.; Chen, P.; Lou, H.; Zheng, X.; Hong, H. Nanostructured molybdenum carbides supported on carbon nanotubes as efficient catalysts for one-step hydrodeoxygenation and isomerization of vegetable oils. *Green Chem.* **2011**, *13*, 2561. [[CrossRef](#)]
15. Hermida, L.; Abdullah, A.Z.; Mohamed, A.R. Deoxygenation of fatty acid to produce diesel-like hydrocarbons: A review of process conditions, reaction kinetics and mechanism. *Renew. Sustain. Energy Rev.* **2015**, *42*, 1223–1233. [[CrossRef](#)]
16. Kay Lup, A.N.; Abnisa, F.; Daud, W.M.A.W.; Aroua, M.K. A review on reaction mechanisms of metal-catalyzed deoxygenation process in bio-oil model compounds. *Appl. Catal. A* **2017**, *541*, 87–106. [[CrossRef](#)]
17. Lestari, S.; Maki-Arvela, P.; Beltramini, J.; Lu, G.Q.; Murzin, D.Y. Transforming triglycerides and fatty acids into biofuels. *ChemSusChem* **2009**, *2*, 1109–1119. [[CrossRef](#)] [[PubMed](#)]

18. Gosselink, R.W.; Hollak, S.A.; Chang, S.W.; van Haveren, J.; de Jong, K.P.; Bitter, J.H.; van Es, D.S. Reaction pathways for the deoxygenation of vegetable oils and related model compounds. *ChemSusChem* **2013**, *6*, 1576–1594. [[CrossRef](#)] [[PubMed](#)]
19. Wagenhofer, M.F.; Baráth, E.; Gutiérrez, O.Y.; Lercher, J.A. Carbon–carbon bond scission pathways in the deoxygenation of fatty acids on transition-metal sulfides. *ACS Catal.* **2017**, *7*, 1068–1076. [[CrossRef](#)]
20. Snåre, M.; Kubičková, I.; Mäki-Arvela, P.; Eränen, K.; Murzin, D.Y. Heterogeneous catalytic deoxygenation of stearic acid for production of biodiesel. *Ind. Eng. Chem. Res.* **2006**, *45*, 5708–5715. [[CrossRef](#)]
21. Lestari, S.; Simakova, I.; Tokarev, A.; Mäki-Arvela, P.; Eränen, K.; Murzin, D.Y. Synthesis of biodiesel via deoxygenation of stearic acid over supported Pd/C catalyst. *Catal. Lett.* **2008**, *122*, 247–251. [[CrossRef](#)]
22. Snåre, M.; Kubičková, I.; Mäki-Arvela, P.; Chichova, D.; Eränen, K.; Murzin, D.Y. Catalytic deoxygenation of unsaturated renewable feedstocks for production of diesel fuel hydrocarbons. *Fuel* **2008**, *87*, 933–945. [[CrossRef](#)]
23. Simakova, I.; Simakova, O.; Mäki-Arvela, P.; Simakov, A.; Estrada, M.; Murzin, D.Y. Deoxygenation of palmitic and stearic acid over supported Pd catalysts: Effect of metal dispersion. *Appl. Catal. A* **2009**, *355*, 100–108. [[CrossRef](#)]
24. Mäki-Arvela, P.; Snåre, M.; Eränen, K.; Myllyoja, J.; Murzin, D.Y. Continuous decarboxylation of lauric acid over Pd/C catalyst. *Fuel* **2008**, *87*, 3543–3549. [[CrossRef](#)]
25. Peng, B.; Zhao, C.; Kasakov, S.; Foraita, S.; Lercher, J.A. Manipulating catalytic pathways: Deoxygenation of palmitic acid on multifunctional catalysts. *Chem. Eur. J.* **2013**, *19*, 4732–4741. [[CrossRef](#)] [[PubMed](#)]
26. Jang, H.; Kim, S.-H.; Lee, D.; Shim, S.E.; Baeck, S.-H.; Kim, B.S.; Chang, T.S. Hydrogenation of lactic acid to propylene glycol over a carbon-supported ruthenium catalyst. *J. Mol. Catal. A Chem.* **2013**, *380*, 57–60. [[CrossRef](#)]
27. Chen, L.; Zhu, Y.; Zheng, H.; Zhang, C.; Zhang, B.; Li, Y. Aqueous-phase hydrodeoxygenation of carboxylic acids to alcohols or alkanes over supported Ru catalysts. *J. Mol. Catal. A Chem.* **2011**, *351*, 217–227. [[CrossRef](#)]
28. Li, W.; Ye, L.; Chen, J.; Duan, X.; Lin, H.; Yuan, Y. Fe-SBA-15-supported ruthenium catalyst for the selective hydrogenolysis of carboxylic acids to alcoholic chemicals. *Catal. Today* **2015**, *251*, 53–59. [[CrossRef](#)]
29. Lugo-José, Y.K.; Monnier, J.R.; Williams, C.T. Gas-phase, catalytic hydrodeoxygenation of propanoic acid, over supported group viii noble metals: Metal and support effects. *Appl. Catal. A* **2014**, *469*, 410–418. [[CrossRef](#)]
30. Chen, J.; Shi, H.; Li, L.; Li, K. Deoxygenation of methyl laurate as a model compound to hydrocarbons on transition metal phosphide catalysts. *Appl. Catal. B* **2014**, *144*, 870–884. [[CrossRef](#)]
31. Bui, P.; Cecilia, J.A.; Oyama, S.T.; Takagaki, A.; Infantes-Molina, A.; Zhao, H.; Li, D.; Rodríguez-Castellón, E.; Jiménez López, A. Studies of the synthesis of transition metal phosphides and their activity in the hydrodeoxygenation of a biofuel model compound. *J. Catal.* **2012**, *294*, 184–198. [[CrossRef](#)]
32. Li, K.; Wang, R.; Chen, J. Hydrodeoxygenation of anisole over silica-supported Ni₂P, MoP, and NiMoP catalysts. *Energy Fuels* **2011**, *25*, 854–863. [[CrossRef](#)]
33. Bowker, R.H.; Smith, M.C.; Pease, M.L.; Slenkamp, K.M.; Kovarik, L.; Bussell, M.E. Synthesis and hydrodeoxygenation properties of ruthenium phosphide catalysts. *ACS Catal.* **2011**, *1*, 917–922. [[CrossRef](#)]
34. Kubička, D.; Kaluža, L. Deoxygenation of vegetable oils over sulfided Ni, Mo and NiMo catalysts. *Appl. Catal. A* **2010**, *372*, 199–208. [[CrossRef](#)]
35. Peng, B.; Yuan, X.; Zhao, C.; Lercher, J.A. Stabilizing catalytic pathways via redundancy: Selective reduction of microalgae oil to alkanes. *J. Am. Chem. Soc.* **2012**, *134*, 9400–9405. [[CrossRef](#)] [[PubMed](#)]
36. Brillouet, S.; Baltag, E.; Brunet, S.; Richard, F. Deoxygenation of decanoic acid and its main intermediates over unpromoted and promoted sulfided catalysts. *Appl. Catal. B* **2014**, *148*, 201–211. [[CrossRef](#)]
37. Ruinat de Brimont, M.; Dupont, C.; Daudin, A.; Geantet, C.; Raybaud, P. Deoxygenation mechanisms on Ni-promoted MoS₂ bulk catalysts: A combined experimental and theoretical study. *J. Catal.* **2012**, *286*, 153–164. [[CrossRef](#)]
38. Toba, M.; Abe, Y.; Kuramochi, H.; Osako, M.; Mochizuki, T.; Yoshimura, Y. Hydrodeoxygenation of waste vegetable oil over sulfide catalysts. *Catal. Today* **2011**, *164*, 533–537. [[CrossRef](#)]
39. Şenol, O.İ.; Ryymin, E.M.; Viljava, T.R.; Krause, A.O.I. Effect of hydrogen sulphide on the hydrodeoxygenation of aromatic and aliphatic oxygenates on sulphided catalysts. *J. Mol. Catal. A Chem.* **2007**, *277*, 107–112. [[CrossRef](#)]

40. Oyama, S.T.; Onkawa, T.; Takagaki, A.; Kikuchi, R.; Hosokai, S.; Suzuki, Y.; Bando, K.K. Production of phenol and cresol from guaiacol on nickel phosphide catalysts supported on acidic supports. *Top. Catal.* **2015**, *58*, 201–210. [[CrossRef](#)]
41. Iino, A.; Cho, A.; Takagaki, A.; Kikuchi, R.; Oyama, S.T. Kinetic studies of hydrodeoxygenation of 2-methyltetrahydrofuran on a Ni₂P/SiO₂ catalyst at medium pressure. *J. Catal.* **2014**, *311*, 17–27. [[CrossRef](#)]
42. Sawhill, S.; Layman, K.; Vanwyk, D.; Engelhard, M.; Wang, C.; Bussell, M. Thiophene hydrodesulfurization over nickel phosphide catalysts: Effect of the precursor composition and support. *J. Catal.* **2005**, *231*, 300–313. [[CrossRef](#)]
43. Franke, R.; Chassé, T.; Streubel, P.; Meisel, A. Auger parameters and relaxation energies of phosphorus in solid compounds. *J. Electron. Spectrosc. Relat. Phenom.* **1991**, *56*, 381–388. [[CrossRef](#)]
44. Landau, M.V.; Herskowitz, M.; Hoffman, T.; Fuks, D.; Liverts, E.; Vingurt, D.; Froumin, N. Ultradeep hydrodesulfurization and adsorptive desulfurization of diesel fuel on metal-rich nickel phosphides. *Ind. Eng. Chem. Res.* **2009**, *48*, 5239–5249. [[CrossRef](#)]
45. Cecilia, J.A.; Infantes-Molina, A.; Rodríguez-Castellón, E.; Jiménez-López, A.; Oyama, S.T. Oxygen-removal of dibenzofuran as a model compound in biomass derived bio-oil on nickel phosphide catalysts: Role of phosphorus. *Appl. Catal. B* **2013**, *136–137*, 140–149. [[CrossRef](#)]
46. Koranyi, T.; Vit, Z.; Poduval, D.; Ryoo, R.; Kim, H.; Hensen, E. SBA-15-supported nickel phosphide hydrotreating catalysts. *J. Catal.* **2008**, *253*, 119–131. [[CrossRef](#)]
47. Oyama, S.T.; Wang, X.; Lee, Y.-K.; Bando, K.; Requejo, F.G. Effect of phosphorus content in nickel phosphide catalysts studied by XAFS and other techniques. *J. Catal.* **2002**, *210*, 207–217. [[CrossRef](#)]
48. Xin, H.; Guo, K.; Li, D.; Yang, H.; Hu, C. Production of high-grade diesel from palmitic acid over activated carbon-supported nickel phosphide catalysts. *Appl. Catal. B* **2016**, *187*, 375–385. [[CrossRef](#)]
49. Chen, Y.; Li, C.; Zhou, J.; Zhang, S.; Rao, D.; He, S.; Wei, M.; Evans, D.G.; Duan, X. Metal phosphides derived from hydrotalcite precursors toward the selective hydrogenation of phenylacetylene. *ACS Catal.* **2015**, *5*, 5756–5765. [[CrossRef](#)]
50. Guan, Q.; Han, F.; Li, W. Catalytic performance and deoxygenation path of methyl palmitate on Ni₂P/SiO₂ synthesized using the thermal decomposition of nickel hypophosphite. *RSC Adv.* **2016**, *6*, 31308–31315. [[CrossRef](#)]
51. Oyama, S.T.; Lee, Y.-K. Bifunctional nature of a SiO₂-supported Ni₂P catalyst for hydrotreating: EXAFS and FTIR studies. *J. Catal.* **2006**, *239*, 376–389. [[CrossRef](#)]
52. Basila, M.I.; Kantner, T.R.; Rhee, K.H. Infrared spectroscopic studies of trimethylamine and pyridine chemisorption. *Nat. Acidic Sites Silica-Alumina* **1964**, *68*, 3197–3207.
53. Wawrzetz, A.; Peng, B.; Hrabar, A.; Jentys, A.; Lemonidou, A.A.; Lercher, J.A. Towards understanding the bifunctional hydrodeoxygenation and aqueous phase reforming of glycerol. *J. Catal.* **2010**, *269*, 411–420. [[CrossRef](#)]
54. Peng, B.; Zhao, C.; Mejía-Centeno, I.; Fuentes, G.A.; Jentys, A.; Lercher, J.A. Comparison of kinetics and reaction pathways for hydrodeoxygenation of C3 alcohols on Pt/Al₂O₃. *Catal. Today* **2012**, *183*, 3–9. [[CrossRef](#)]
55. Fu, J.; Lu, X.; Savage, P.E. Catalytic hydrothermal deoxygenation of palmitic acid. *Energy Environ. Sci.* **2010**, *3*, 311–317. [[CrossRef](#)]
56. Li, W.; Gao, Y.; Yao, S.; Ma, D.; Yan, N. Effective deoxygenation of fatty acids over Ni(OAC)₂ in the absence of H₂ and solvent. *Green Chem.* **2015**, *17*, 4198–4205. [[CrossRef](#)]

